J. Radiat. Res., 51, 723–731 (2010)

Regular Paper

Investigation on Effect of Image Lag in Fluoroscopic Images Obtained with a Dynamic Flat-panel Detector (FPD) on Accuracy of Target Tracking in Radiotherapy

Rie TANAKA[1]*, Katsuhiro ICHIKAWA[1], Shinichiro MORI[2], Suguru DOBASHI[2], Motoki KUMAGAI[2], Hiroki KAWASHIMA[3], Shinichi MINOHARA[2] and Sigeru SANADA[1]

Target tracking/Image lag/Fluoroscopic image/Flat-panel detector (FPD)/Radiotherapy.

Real-time tumor tracking in external radiotherapy can be achieved by diagnostic (kV) X-ray imaging with a dynamic flat-panel detector (FPD). The purpose of this study was to address image lag in target tracking and its influence on the accuracy of tumor tracking. Fluoroscopic images were obtained using a direct type of dynamic FPD. Image lag properties were measured without test devices according to IEC 62220-1. Modulation transfer function (MTF) and profile curves were measured on the edges of a moving tungsten plate at movement rate of 10 and 20 mm/s, covering lung tumor movement of normal breathing. A lung tumor and metal sphere with blurred edge due to image lag was simulated using the results and then superimposed on breathing chest radiographs of a patient. The moving target with and without image lag was traced using a template-matching technique. In the results, the image lag for the first frame after X-ray cutoff was 2.0% and decreased to less than 0.1% in the fifth frame. In the measurement of profile curves on the edges of static and moving tungsten material plates, the effect of image lag was seen as blurred edges of the plate. The blurred edges of a moving target were indicated as reduction of MTF. However, the target could be traced within an error of ± 5 mm. The results indicated that there was no effect of image lag on target tracking in usual breathing speed in a radiotherapy situation.

INTRODUCTION

Real-time tumor tracking in external radiotherapy can be achieved by diagnostic (kV) X-ray imaging with a dynamic flat-panel detector (FPD).[1–3] These FPD systems are expected to solve the problems of low image contrast and quality seen in megavoltage imaging. However, there are still a number of factors that reduce the accuracy of target tracking in external radiation therapy. In terms of image quality, image lag, ghosting, image noise, contrast, and resolution are thought to effect on the accuracy of tracking. Image lag and ghosting which may induce blurring on the contours of a moving target, especially need a lot of attention. Lag is the carryover of image charge generated by previous X-ray exposures into subsequent image frames. Ghosting is the change of X-ray sensitivity, or gain, of the detector as a result of previous radiation exposure. Lag and ghosting in a-Se FPDs are determined by the properties of both the a-Se layer and the active matrix.[4,5] Previous studies indicated that primary a-Se FPDs showed a lag in the first frame after X-ray exposure of less than 5%.[6–9] Modifications in the technology of the a-Se detectors appear to have resulted in marked decreases in both lag and ghosting effects in more recent systems.[10–12] Recently, several methods for measuring temporal modulation transfer function (MTF) and detective quantum efficiency (DQE) have been proposed and the properties of FPDs used in dynamic imaging have been reported.[13–15] However, there have been no studies regarding image qualities affect motion tracking by dynamic imaging with FPDs. In external radiotherapy, there is concern regarding the relationship between image quality and total patient dose during real-time tumor tracking, because it is necessary to optimize imaging parameters in each patient to keep patient dose as low as possible while maintaining tracking

*Corresponding author: Phone: +81-76-265-2537,
Fax: +81-76-234-4366,
E-mail: rie44@mhs.mp.kanazawa-u.ac.jp
[1]Department of Radiological Technology, School of Health Sciences, College of Medical, Pharmaceutical and Health Sciences, Kanazawa University; 5-11-80 Kodatsuno, Kanazawa, 920-0942, Japan; [2]Research Center for Charged Particle Therapy, National Institute of Radiological Sciences; 4-9-1 Anagawa, Inage-ku, Chiba, 263-8555, Japan; [3]Department of Radiology, Kanazawa University Hospital; 13-1 Takara-machi, Kanazawa, 920-8641, Japan.
doi:10.1269/jrr.10059

accuracy. Here, we investigated image lag and MTF during target tracking in external radiotherapy. The purpose of this study was to address its influence on the accuracy of tumor tracking.

MATERIALS AND METHODS

Imaging devices and geometry

Dynamic images were obtained using a dynamic FPD system (SONIALVISION SafireII; Shimadzu, Kyoto, Japan). The system was developed for real-time target tracking in three dimensions for external radiotherapy and it was limited to 1.0 m in the source-to-image distance (SID) (Fig. 1). The FPD was a direct type consisting of an a-Se/TFT imaging array and the maximum imaging rate was 30 frames per second (fps). In this study, one of the FPDs was examined. The experiments were performed according to IEC 62220-1 standard.[16] The matrix size was 1024 × 1024 pixels, the pixel size was 248 × 248 μm, field of view was 25.4 × 25.4 cm, and the grayscale range of the images was 16 bits, which was proportional to the incident exposure in the FPD.

Lag measurement

Lag measurement experiments were performed at a standard X-ray spectrum without grid (IEC RQA5; 70 kV, 23 mA, 4 ms, 3.2 mR). After irradiation more than 10 times, the X-ray was cutoff and images continued to be read out and stored. IEC 62220-1-3 standard shows two requirements in the number of stored images; one is a power of 2 and the other is stable mean pixel value in the obtained images, and recommends acquisition of 64 images.[17] However, in the present study, 32 images were stored due to system limitations. Note that the image sets were confirmed to fulfill the requirements, *i.e.,* stability of mean pixel values. The region of interest (ROI) measuring 256 × 256 pixels was located manually on the detector center and average pixel value was measured using Image-J ver. 1.42 (http://rsb.info.nih.gov/ij/) (Fig. 2). Image lag can be defined as the carryover of trapped charge generated by X-ray exposure into subsequent image frames acquired with no X-ray exposure, and that in the *n*th frame (L_n) can be calculated as follows:[4]

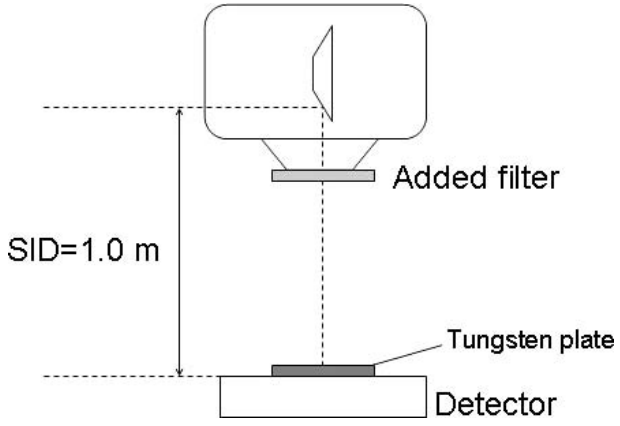

Fig. 1. Geometry of the FPD system evaluated in this study. Added filter and a tungsten plate were set in contact with the X-ray tube and the detector surface, respectively. Source-to-image distance was limited to 1.0 m in the system which was evaluated in this study.

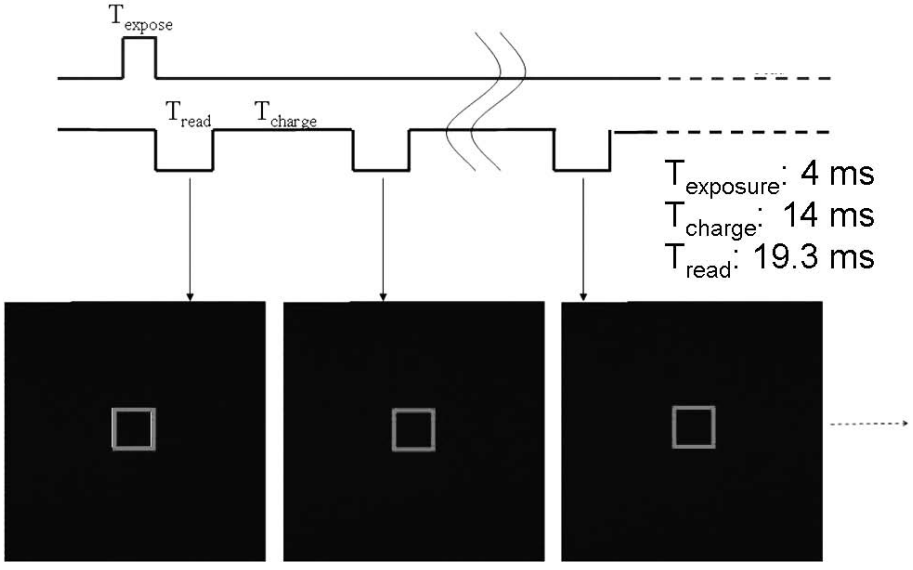

Fig. 2. Imaging chart and images obtained. Images were read after exposure. The squares show the region of interest (ROI) for measuring pixel values to determine image lag. $T_{exposure}$, T_{charge}, and T_{read} are the time for exposing X-ray, charging and reading electric charge, respectively.

$$L_n = \left(\frac{S_n - B}{S_0 - B} \right) \times 100 \quad (1)$$

where S_n and S_0 are the average pixel values measured in ROI in frame number n and the 0^{th} frame acquired immediately following X-irradiation and cutoff, respectively. The term B is the pixel value measured in the background image, which was obtained without any radiation. Three sets of images were evaluated and the average L_n value was calculated in each nth frame from X-ray cutoff.

MTF measurement

A tungsten plate with a precision edge (thickness, 1 mm; size, 10 × 10 cm; IEC standard) was mounted onto a motor control device, which provided a constant velocity. The plate was positioned in such a way that the edge was slightly (~2°) tilted with respect to the axis of the image matrix.[16] The plate was moved into the detector in contact with the detector surface. Figure 3 shows imaging chart and images of a tungsten plate. The movement rate was 10 and 20 mm/s, covering lung tumor movement of normal breathing. Imaging was performed under conditions of target tracking in external radiotherapy in our center (15 fps, 70 kV, 23 mA, 4 ms). Images of the static plate were also obtained for comparison between the results in dynamic and static states. In the present study, the edge in the direction of movement was referred to as the "edges covering the detector," and those in the opposite side were referred to as the "edges uncovering the detector." Profile curves of average pixel values in 50 rows were obtained in both edges covering and uncovering the detector, to evaluate image blurring visually and quantitatively. Subsequently, ROIs of 256 × 256 pixels were located on the edges covering and uncovering the detector. The frame with the edge closest to the detector center was used to calculate the MTF. For determination of MTF, the method given in the IEC standard was used.[16] The standard process of derivation of the edge spread function (ESF) to obtain the line spread function (LSF) and subsequent fast Fourier transform to obtain the presampled MTF was applied. The measurement was performed by using the analysis tool kit, which was provided in the digital radiography seminar held by image research group of Japanese society of radiological technology.

Creation of simulated images

(i) Creation of a target

A digitally generated lung nodule and metal sphere were used as a target in this study. The phantom of the lung nodule was created based on Gaussian distribution as follows:

$$f(x) = \frac{1}{\sqrt{2\pi}\sigma} \exp\left(-\frac{(x-\mu)^2}{2\sigma^2}\right) \quad (0 \le x < X) \quad (2)$$

where x is the distance from the center of the Gaussian distribution, μ is the mean displacement and σ is the standard deviation. In this study, X and σ were 120 and 25 pixels, respectively, to create a round target of 1 cm in diameter at 75% value width, and μ was determined by multiplying the

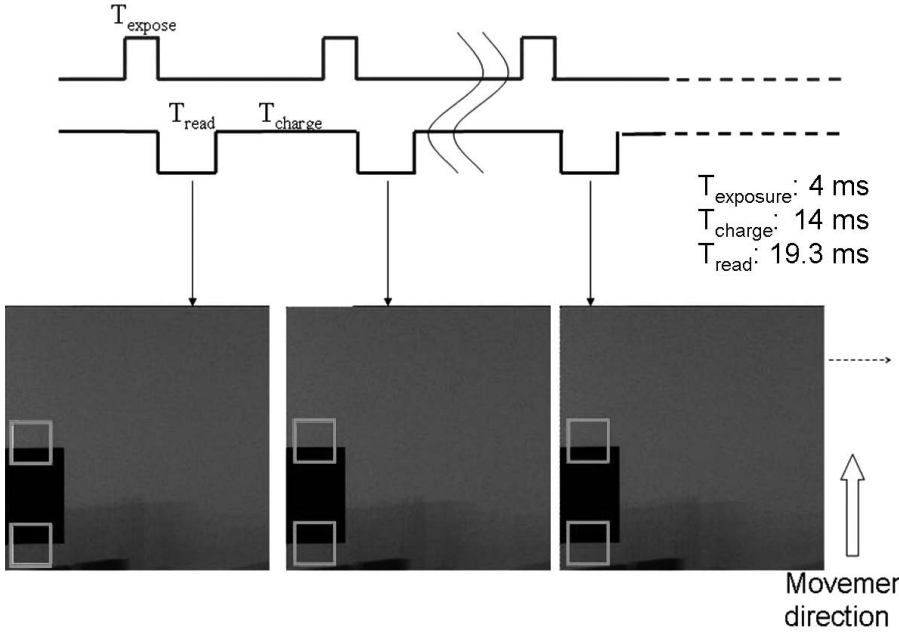

Fig. 3. Imaging chart and images of a moving tungsten plate (70 kV, 1.4 mAs, 15 fps, attached Al filter 4 mm). The squares show the region of interest (ROI) to measure MTF. $T_{exposure}$, T_{charge}, and T_{read} are the time for exposing X-ray, charging and reading electric charge, respectively.

process number of frames and a movement rate in units of pixels/frame. The target inserted onto a chest radiographs was observed as a round tumor of about 1 cm in diameter. The targets moving at rates of 10 mm/s and 20 mm/s were displaced by 2.7 and 5.4 pixels/frame, respectively. The target in the nth frame $T(n)$ is described as:

$$T(n) = P \times f(x), \tag{3}$$

where P is the pixel value at the center of the target, which was determined based on the pixel value of soft tissues

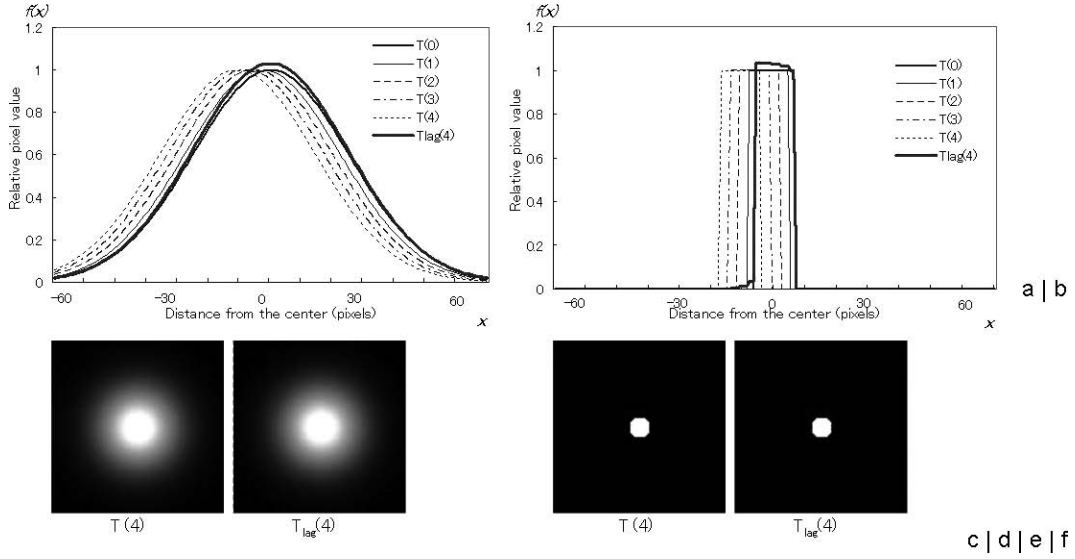

Fig. 4. Process of creating a digital phantom. (a) The lung tumor of 1 cm in diameter with image lag, moving at a rate of 10 mm/s ($X = 120$, $\sigma = 25$, $\mu = 2.7 \times k$, $0 < k < 5$), with half bandwidth of the distribution given by 60 pixels, and (b) a metal sphere of 3 mm in diameter, with a well-defined edge. The bold and solid lines show simulated target with image lag ($n = 4$), $T_{lag}(4)$. Results image of the lung tumor (c) without and (d) with image lag, and a metal sphere (e) without and (f) with image lag, respectively. The direction of movement is diagonally downward to the right.

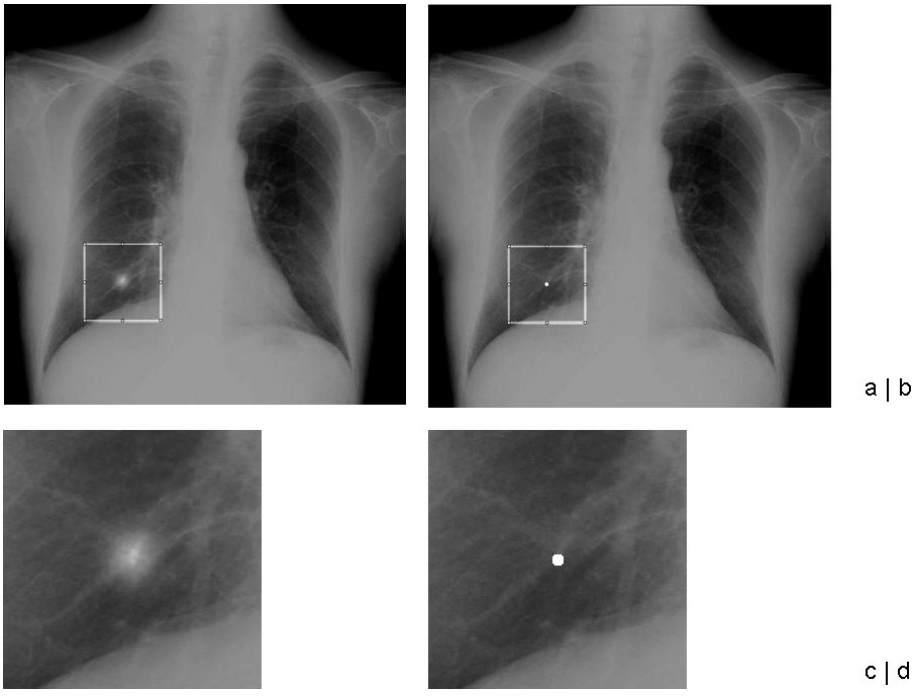

Fig. 5. Simulated images with (a) a lung tumor and (c) a metal sphere in the right lower lung (n = 0) and the enlarged images of (c) the lung tumor and (d) the metal sphere surrounded by the solid squares.

around the insert position. In addition, to investigate an influence of the target shape on the accuracy of target tracking, the digital phantom of metal sphere was created as a circle with a well-defined edge, high pixel value, and 3 mm in diameter.

(ii) Simulation of image lag

A moving target in the nth frame $T_{lag}(n)$ was simulated using the results of lag measurement as follows:

$$T_{lag}(n) = T(n) + \sum_{k} \{T(n-k) \times L_k\} \quad (4)$$

where k is the frame number going back from the n^{th} frame of interest, and L_k is the image lag (%) calculated by Eq. (1). The computation was repeated while L_k was greater than 0.1. Figures 4a and 4b show the process of creating a target with image lag. Figures 4c to 4f show targets with and without image lag created by this method.

(iii) Creation of target trajectory

The images of the lung nodule and metal sphere were digitally added into chest images of a patient during respiration obtained with the FPD system, as shown in Figs. 5a and 5b, respectively. Approval for the study was obtained from our institutional review board, and the subjects gave written informed consent prior to participation. The path of the target was determined based on the distinguishable shadows of pulmonary vessels around the position where the digital lung nodule and metal sphere were inserted in the image. Figure 6 shows the trajectory of the shadows of pulmonary vessels in the lower right lung, which was measured manually by one medical physicist (R.T.) with clinical experience in diagnostic imaging. The measurements were performed three times and the average was adopted as the benchmark in the evaluation of the accuracy in target tracking. The movement speed was simulated in two patterns, 10 mm/s and 20 mm/s, covering the range of lung tumor movement in normal breathing.

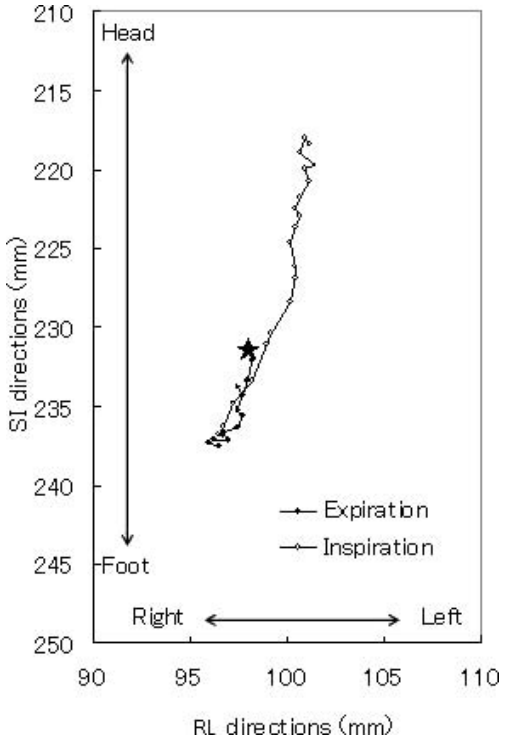

Fig. 6. Trajectory of target determined based on the distinguishing shadows of pulmonary vessels around the inserted target on breathing chest radiographs. In this study, it was measured in the right lower lung. The path was given to simulated target. The star indicates frame #. 0. (SI: Superior to Inferior, RL: Right to Left).

Trace of a moving target

The targets in the simulation images were tracked by a template-matching technique.[18] The targets without background image were also evaluated to investigate influence of the background images. The summation of differences in pixel value (R) between the search area in the next frame, $S(x + dx, y + dy)$, and template in the current frame, $T(x, y)$, was expressed as follows:

$$R = \sum_{y=0}^{N} \sum_{x=0}^{M} \left| S(x+dx, y+dy) - T(x,y) \right| \quad (5)$$

$$(0 < x < M,\ 0 < y < N,\ -10 < dx < 10,\ -10 < dy < 10)$$

M and N are the size of the template, and dx and dy are the search range. The smallest R value was obtained when there were more similarities in the search area and template. The amount of shift (dx, dy) in the search area was determined by minimizing R, and the coordinates after movement were expressed as ($x + dx$, $y + dy$). In this study, the initial template was defined as the region around which the target was inserted in the first frame. From the second frame onwards, the matching region of interest in the previous frame was used as the new template.

In tracing the tumor target, the size of the template used was 100 × 100 with a search range of ± 10 pixels, resulting in a search area of 120 × 120 pixels. This was determined based on the movement rate of the target and a constant value during tracking. While, in trace of a metal sphere target, the size of template was 50 × 50 pixels, which was the size enough to cover the target. The targets moving at rates of 10 mm/s and 20 mm/s were displaced by 2.7 pixels/frame and 5.4 pixels/frame, respectively. The displacements were sufficiently covered by a search range of ± 10 pixels.

Data analysis

Four image sets with a moving target were assessed in the present study at 10 mm/s or 20 mm/s with and without image lag in each target, the lung tumor and metal sphere. The targets were tracked automatically and compared with the benchmark, the results of manual tracking. Tracking errors were calculated as differences between "the results of

automatic tracking" and "the benchmark" to evaluate the influence of blurring due to image lag on the accuracy of target tracking.

RESULTS

Image lag properties

Figure 7a shows the average pixel values measured in the ROIs. The average pixel values were reduced immediately after X-ray cutoff and reached the minimum value in the fifth (n = 5) frame after X-ray cutoff. Subsequently, they increased slightly and achieved a stable state at the end of the image sequence. Figure 7b shows image lag (L_n) for frame n = 0 through n = 9. The image lag for the first (n = 1), second (n = 2), third (n = 3), and fourth (n = 4) frames after X-ray cutoff were 2.0%, 0.85%, 0.37%, and 0.10%, respectively, and dropped to less than 0.10% in the fifth (n = 5) frame after X-ray cutoff.

MTF properties and edge profile curves

Figure 8 shows the profile curves obtained on the edges of a tungsten plate. From the profile, the edges were steep slopes composed of three to four pixels and the slopes of the moving plate were more gradual than those of the static

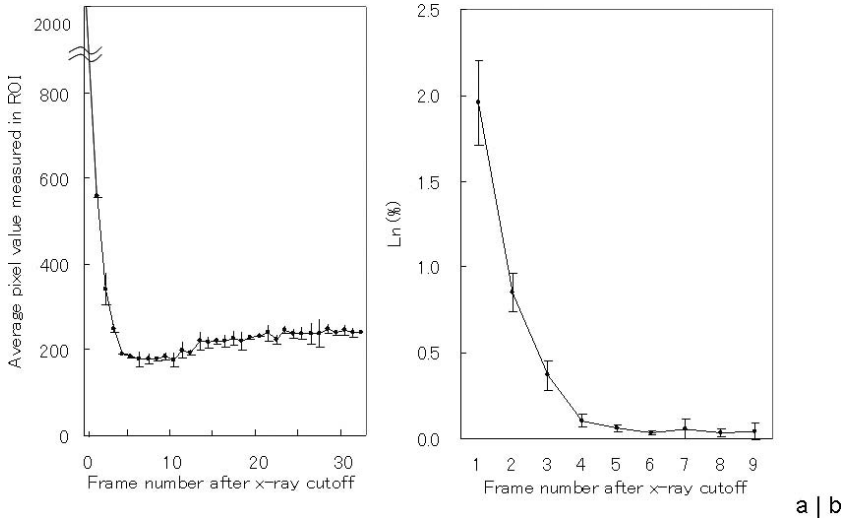

Fig. 7. Image Lag properties. (a) Average pixel values measured in the ROIs. (b) L_n for frame n = 0 through n = 9. Error bars show ± SD (N = 3).

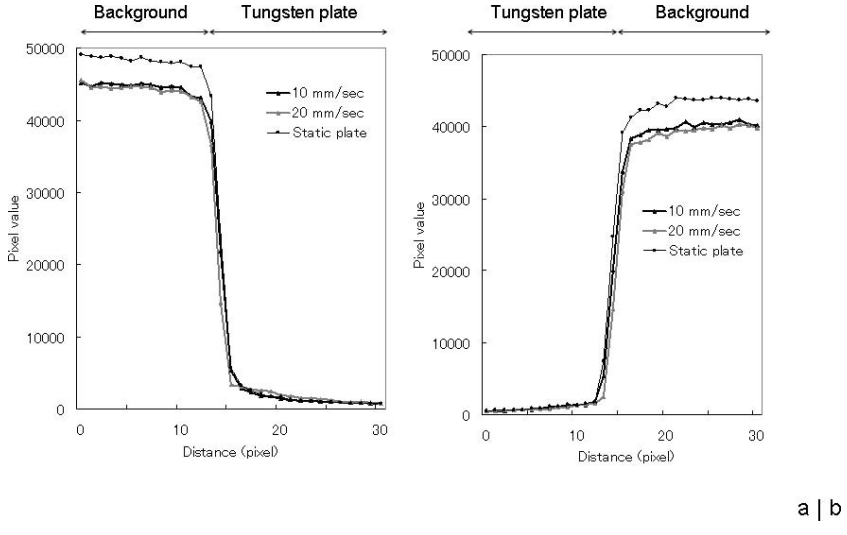

Fig. 8. Profile curves obtained on edges of a tungsten plate (a) covering and (b) uncovering the detector. *The edge in the direction of movement is referred to as the "edges covering the detector," and those in the opposite side is referred to as the "edges uncovering the detector."

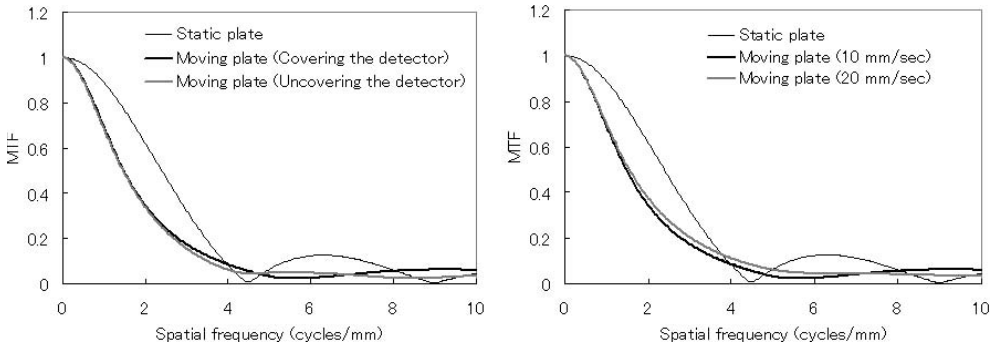

Fig. 9. (a) MTF of static and moving tungsten plate on an edge covering and uncovering the detector (10 mm/s), (b) MTF of static and moving tungsten plate on an edge covering the detector (10 mm/s and 20 mm/s).

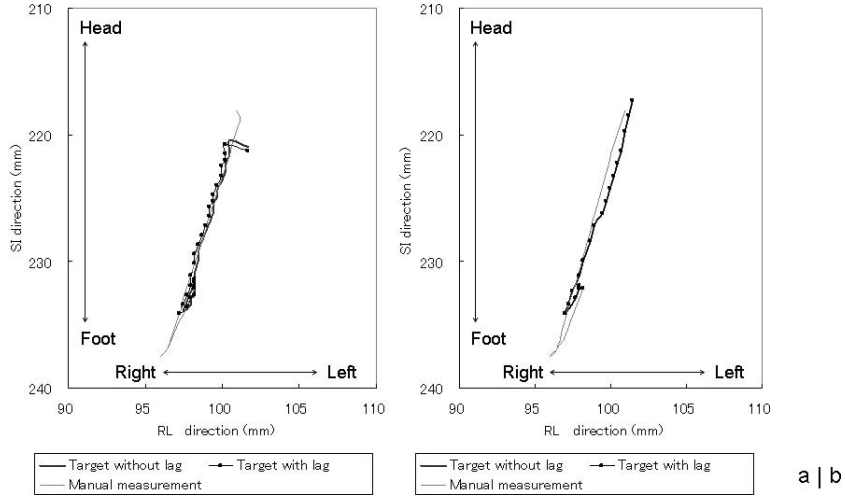

Fig. 10. Results of automatic tracking of a moving lung tumor with and without image lag at a rate of (a) 10 mm/s and (b) 20 mm/s. (SI: Superior to Inferior, RL: Right to Left).

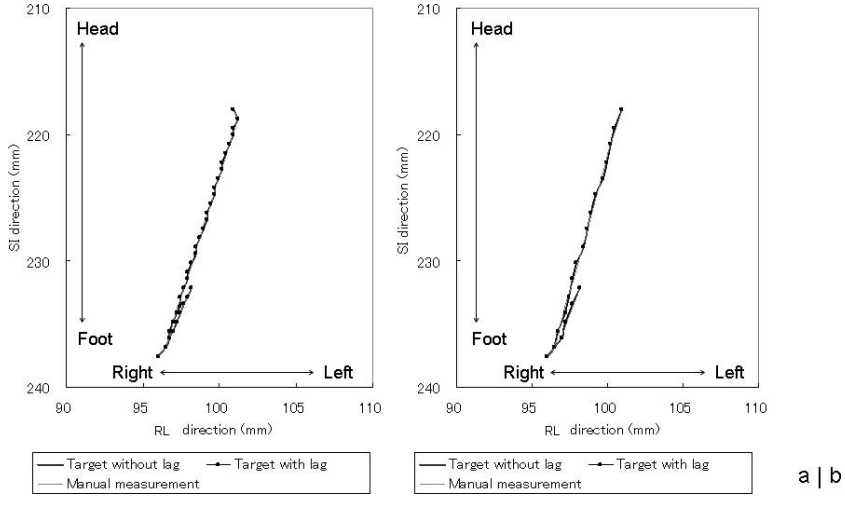

Fig. 11. Results of automatic tracking of a moving metal sphere with and without image lag at a rate of (a) 10 mm/s and (b) 20 mm/s. (SI: Superior to Inferior, RL: Right to Left).

plate. There was no visible difference between the edges of plate covering and uncovering the detector. There was also no significant difference in the profile curves at rates of 10 mm/s and 20 mm/s. Figure 9a shows the MTF of a static tungsten plate and a plate moving at a rate of 10 mm/s. The results indicated that the present FPD system had good MTF properties which were equivalent to the results reported by the previous study.[13–15] The MTF of a moving plate was much lower than that of a static plate; however, there was no significant difference between the edges of the plate covering and uncovering the detector. Figure 9b shows the MTF measured on the covering edge of a static tungsten material plate and plates moving at rates of 10 mm/s and 20 mm/s. There were also no significant differences in MTF of a target moving at rates of 10 mm/s and 20 mm/s. The results obtained by measurement of edge profile curves were supported by the MTF measurements, as shown in Figs. 9.

Effects of image lag on target tracking

The target could be traced within a margin for error (± 5 mm) in external radiotherapy. Figure 10a shows the results of the automatic tracking of a moving tumor target with and without image lag at a rate of 10 mm/s. The maximum tracking errors of a target with and without image lag were 4.2 mm and 4.5 mm, respectively. Figure 10b shows the results in a target moving at a rate of 20 mm/s. The maximum errors in tracking target were 3.5 mm for both targets with and without image lag. In addition, those without background images were 0.25 mm, for both targets with and without image lag, at a rate of 10 mm/s and 20 mm/s. Figures 11 show the results in a simulated metal sphere. The tracking error was less than the pixel size and very small, with and without image lag, at a rate of 10 mm/s and 20 mm/s, with and without background images, with and without background images.

DISCUSSION

There are a number of factors that reduce the accuracy of target tracking in external radiation therapy. In terms of image quality, image lag, noise, contrast, and resolution are thought to affect on the accuracy of tracking. In the present study, we investigated image lag properties of a dynamic FPD system in target tracking for external radiotherapy. The image lag for the first frame (n = 1) after X-ray cutoff was 2.0% and decreased to less than 0.1% in the fifth frame in our direct type dynamic FPD system. These results were consistent with those reported by other groups.[10–12] In the measurement of profile curves on the edges of static and moving tungsten material plates, the effect of image lag was seen as blurred edges of the plate. In the MTF measurement, the blurred edges of a moving target were indicated as reduction of MTF. In the present study, there were no visible or significant differences in the profile curves and MTF between movement rates of 10 mm/s and 20 mm/s, or between edges of a moving plate covering and uncovering the detector. The results suggested that there is no need to consider contour blurring due to image lag under normal breathing at the imaging rate of 15 fps. However, to address the threshold of movement rate that impacts target tracking, further studies involving various movement rates and imaging rates are needed.

The lag property, reduction of MTF and visible contour blurring of a moving target potential sources of errors in target tracking in external radiotherapy, *i.e.*, out of track due to false detection of the target. In the simulation experiment, however, all motion targets created using such lag properties could be tracked within an error of ± 5 mm, which is less than overall spatial uncertainty in external radiotherapy.[19] In addition, there were no significant differences in maximum error between targets with and without image lag. The results indicated that image lag had only negligible effect on target tracking in external radiation therapy. This can be accountable for by the fact that there are only a few pixels of interframe movement of the target under normal conditions of quiet breathing during radiotherapy. The present results suggested that, factors other than image lag, such as image noise, contrast, and resolution, would have greater deleterious effects on tracking accuracy. While, there were differences in maximum error between target types. Thus, further studies are required to investigate the influences of target shape, size, and its density on the accuracy of target tracking.

There was a problem in the results of tracking a tumor in simulated images. Although the maximum errors were within the acceptable range, accuracy was not satisfactory. In addition, the maximum error was slightly larger in a target without than with lag. This was thought to be because motion of target was simulated based on trajectories of shadows around the inserted target. To give a constant movement rate to the target through all frames, such as 10 mm/s or 20 mm/s, there may be some differences in the movement between a simulated target and the other shadows, including the template. Such conditions often result in tracking errors. It is also supported by the results that the maximum errors in a tumor inserted chest images were more than those without background images. Simulation method should be improved for more accurate evaluations.

In conclusion, we investigated image lag propertis of a dynamic FPD system under conditions of target tracking in external radiotherapy. Image lag properties were assessed and a moving target with image lag was simulated using the results. The simulated target was tracked within an error of ± 5 mm. In addition, there was no significant difference between the target with and without image lag. The results indicated that there was no effect of image lag on target tracking in external radiation therapy. Further studies are required to investigate the effect of a variety of parameters,

such as tube voltage, image noise, imaging rate, target shape, and thickness of the patient's body.

REFERENCES

1. Jaffray DA, *et al* (2002) Flat-panel cone-beam computed tomography for image-guided radiation therapy. Int J Radiat Oncol Biol Phys **53**: 1337–1349.
2. Moore CJ, *et al* (2006) Developments in and experience of kilovoltage X-ray cone beam image-guided radiotherapy. Br J Radiol **79**: 66–78.
3. Huntzinger C, *et al* (2006) Dynamic targeting image-guided radiotherapy. Med Dosim **31**: 113–125.
4. Zhao W, Degrescenzo G and Rowlands JA (2002) Investigation of lag and ghosting in amorphous selenium flat-panel detectors. SPIE medical imaging. Proc SPIE **4682**: 9–20.
5. Bloomquist AK, *et al* (2006) Lag and ghosting in a clinical flat-panel selenium digital mammography system. Med Phys **33**: 2998–3005.
6. Siewerdsen JH and Jaffray DA (1999) A ghost story: Spatio-temporal response characteristics of an indirect detection flat-panel imager. Med Phys **26**: 1624–1641.
7. Choquette M, *et al* (2000) Direct selenium x-ray detector for fluoloscopy, R&F, and radiography. SPIE medical imaging. Proc SPIE **3977**: 128–136.
8. Adachi S, *et al* (2000) Experimental evaluation of a-Se and CdTe flat-panel detectors for digital radiography and fluoroscopy. SPIE medical imaging. Proc SPIE **3977**: 38–47.
9. Schroeder C, *et al* (2004) Lag measurement in an a-Se active matrix flat-panel imager. Med Phys **31**: 1203–1209.
10. Pokischuk B, *et al* (1998) Selenium direct converter structure for static and dynamic x-ray detection in medical imaging applications. SPIE medical imaging. Proc SPIE **3336**: 494–504.
11. Lee DL, *et al* (1998) Improved imaging performance of 14 × 17-inch direct radiography system using Se/TFT detector. SPIE medical imaging. Proc SPIE **3336**: 14–23.
12. Tsukamoto A, *et al* (1999) Development and evaluation of a large-area selenium-based flat panel detector for real-time radiography and fluoroscopy. SPIE medical imaging. Proc SPIE **3659**: 14–23.
13. Overdick M, Solf T and Wischmann H (2001) Temporal artifacts in flat dynamic x-ray detectors. SPIE medical imaging. Proc SPIE **4320**: 47–58.
14. Friedman SN and Cunningham IA (2006) A Method to measure the temporal MTF to determine the DQE of fluoroscopy system. SPIE medical imaging. Proc SPIE **6142**: 61421X-1-61421X-11.
15. Friedman SN and Cunningham IA (2009) A small-signal approach to temporal modulation transfer functions with exposure-rate dependence and its application to fluoroscopic detective quantum efficiency. Med Phys **36**: 3775–3785.
16. Determination of the detective quantum efficiency (2003) In: IEC International standard 62220-1. Medical diagnostic X-ray equipment-Characteristics of digital imaging devices-Part 1. Geneva, International electrotechnical commission.
17. Determination of the detective quantum efficiency – detectors used in dynamic imaging (2008) In: IEC International standard 62220-1. Medical diagnostic X-ray equipment-Characteristics of digital imaging devices-Part 3 Geneva, International electrotechnical commission.
18. Ballard DH and Brown CM (1982) VII Motion. In: Computer vision. pp. 195–225. Englewood Cliffs, New Jersey, Prentice-hall.
19. Klein EE, *et al* (2009) Task Group 142 report: Quality assurance of medical accelerators. Med Phys **36**: 4197–4212.

Received on May 13, 2010
Revision received on August 27, 2010
Accepted on September 7, 2010
J-STAGE Advance Publication Date: October 23, 2010